

---

This is an electronic reprint of the original article.  
This reprint may differ from the original in pagination and typographic detail.

Neuvonen, P.T.; Vines, L.; Venkatachalapathy, V.; Zubiaga, A.; Tuomisto, F.; Hallén, A.; Svensson, B.G.; Kuznetsov, A.Yu

## Defect evolution and impurity migration in Na implanted ZnO

*Published in:*  
Physical Review B

*DOI:*  
[10.1103/PhysRevB.84.205202](https://doi.org/10.1103/PhysRevB.84.205202)

Published: 01/11/2011

*Document Version*  
Publisher's PDF, also known as Version of record

*Please cite the original version:*

Neuvonen, P. T., Vines, L., Venkatachalapathy, V., Zubiaga, A., Tuomisto, F., Hallén, A., Svensson, B. G., & Kuznetsov, A. Y. (2011). Defect evolution and impurity migration in Na implanted ZnO. *Physical Review B*, 84(20), 1-7. Article 205202. <https://doi.org/10.1103/PhysRevB.84.205202>

---

This material is protected by copyright and other intellectual property rights, and duplication or sale of all or part of any of the repository collections is not permitted, except that material may be duplicated by you for your research use or educational purposes in electronic or print form. You must obtain permission for any other use. Electronic or print copies may not be offered, whether for sale or otherwise to anyone who is not an authorised user.

## Defect evolution and impurity migration in Na-implanted ZnO

Pekka T. Neuvonen,<sup>1,\*</sup> Lasse Vines,<sup>1</sup> Vishnukanthan Venkatachalapathy,<sup>1</sup> Asier Zubiaga,<sup>2</sup> Filip Tuomisto,<sup>2</sup> Anders Hallén,<sup>3</sup> Bengt G. Svensson,<sup>1</sup> and Andrej Yu. Kuznetsov<sup>1</sup>

<sup>1</sup>*Department of Physics, Centre for Material Science and Nanotechnology, University of Oslo, P.O. Box 1048 Blindern, NO-0316 Oslo, Norway*

<sup>2</sup>*Department of Applied Physics, Aalto University, P.O. Box 11100, FI-00076 Aalto, Finland*

<sup>3</sup>*Royal Institute of Technology, School of ICT, Dept. of Microelectronics and Applied Physics, P.O. Box Electrum 229, SE-164 40 Kista, Sweden*

(Received 10 June 2011; revised manuscript received 9 September 2011; published 3 November 2011)

Secondary ion mass spectrometry (SIMS) and positron annihilation spectroscopy (PAS) have been applied to study impurity migration and open volume defect evolution in Na<sup>+</sup> implanted hydrothermally grown ZnO samples. In contrast to most other elements, the presence of Na tends to decrease the concentration of open volume defects upon annealing and for temperatures above 600 °C, Na exhibits trap-limited diffusion correlating with the concentration of Li. A dominating trap for the migrating Na atoms is most likely Li residing on Zn site, but a systematic analysis of the data suggests that zinc vacancies also play an important role in the trapping process.

DOI: [10.1103/PhysRevB.84.205202](https://doi.org/10.1103/PhysRevB.84.205202)

PACS number(s): 81.05.Dz, 61.72.uj, 66.30.J-, 61.72.Cc

### I. INTRODUCTION

Zinc oxide (ZnO) is a direct wide band-gap ( $\sim 3.4$  eV) semiconductor with high exciton binding energy ( $\sim 60$  meV)<sup>1</sup> making it highly desirable for optoelectronic devices, such as light emitting diodes, UV sources/sensors, room-temperature (RT) lasers,<sup>2,3</sup> etc. Recent developments in growth of ZnO<sup>4,5</sup> have made high-quality single crystalline wafers available, giving ZnO an advantage over more traditional direct wide band-gap materials, e.g., nitrides. ZnO wafers exhibit native *n*-type conductivity, although its origin is still under debate. Intrinsic defects, like zinc interstitials (Zn<sub>i</sub>) and oxygen vacancies (V<sub>O</sub>) have been suggested as responsible for the native *n*-type conductivity,<sup>6–8</sup> whilst other reports state that the formation energy of Zn<sub>i</sub> is too high,<sup>9</sup> and the donor level of V<sub>O</sub> is too deep<sup>10</sup> to explain the native conductivity. Moreover, different impurities, such as Al, Ga, In, and H are incorporated into ZnO during growth and can act as shallow donors.<sup>11–13</sup> However, none of these impurities alone can account for the donor concentrations observed suggesting contributions from different donorlike defects and impurities.<sup>14</sup>

The major obstacle challenging the realization of bipolar ZnO devices is the unreliable *p*-type doping, which has much in common with those known for other wide band-gap semiconductors:<sup>15,16</sup> (i) acceptor-type dopants exhibit solid solubility below typical native donor concentrations, (ii) acceptors states are deep in the band gap preventing sufficient ionization at RT, or (iii) dopants adopt several configurations in the lattice leading to self-compensation. In particular, atomic configurations of Li and Na in ZnO depend on the position of the Fermi level ( $E_F$ ); for  $E_F$  close to the conduction band edge, Li (Na) atoms on substitutional sites—Li<sub>Zn</sub> (Na<sub>Zn</sub>)—prevail, while Li (Na) atoms on interstitial sites—Li<sub>i</sub> (Na<sub>i</sub>)—are favoured when  $E_F$  is close to the valence band edge.<sup>17,18</sup> Thus, in *n*-type hydrothermally grown (HT) ZnO, which contains  $\gtrsim 10^{17}$  Li/cm<sup>3</sup>, the predominant configuration is Li<sub>Zn</sub>, often resulting in highly resistive material.<sup>19,20</sup>

In this study, the interaction between Li and Na has been investigated by implanting Na into (i) HT samples

with a Li content of  $\sim 4 \times 10^{17}$  cm<sup>-3</sup> and (ii) HT samples subjected to postgrowth anneals reducing the Li content to the  $10^{15}$  cm<sup>-3</sup> range. Especially, secondary ion mass spectrometry (SIMS) and positron annihilation spectroscopy (PAS) have been combined to reveal the role of zinc vacancies (V<sub>Zn</sub>) in the interaction between Li and Na.

### II. EXPERIMENTAL

Four initially high-resistive (*n* type,  $\rho \sim 1$  kΩcm)  $10 \times 10$  mm HT ZnO wafers, labeled A–D and containing  $2\text{--}4 \times 10^{17}$  Li/cm<sup>3</sup> (called HT Li level), were used. Wafers C and D were heat treated before ion implantation (preannealed) at 1500 °C to reduce the amount of Li by at least two orders of magnitude.<sup>19</sup> Note that the preannealing causes an increase in the Na background concentration from  $< 10^{15}$  cm<sup>-3</sup> (wafers A and B) to the  $10^{16}$  cm<sup>-3</sup> range (wafers C and D) due to furnace contamination. A standard mechanical polishing process using diamond slurry with grain size from 5 μm down to 0.25 μm on rotating nylon suspension disks followed the preanneals of the wafers C and D in order to restore the surface quality. Na implants were performed at RT with an energy of 150 keV resulting in a projected range ( $R_p$ ) of  $\sim 180$  nm. A 7° tilt angle relative to the incident ion beam was used to reduce channeling effects. Wafers A and C were subjected to a dose of  $1 \times 10^{14}$  Na/cm<sup>2</sup> and wafers B and D to  $1 \times 10^{15}$  Na/cm<sup>2</sup>. After implantation, the wafers were cut into four pieces labeled as a wafer quarter, e.g., A.1 and A.2, and then annealed in oxygen ambient under different conditions, as summarized in Table I.

Li and Na concentration versus depth profiles were measured by secondary ion mass spectrometry (SIMS) using a Cameca IMS7f microanalyzer. A primary beam of 10 keV O<sub>2</sub><sup>+</sup> ions was rastered over a  $125 \times 125$  μm<sup>2</sup> surface area and secondary ions were collected from central region of the sputtered crater. Crater depths were measured with a Dektak 8 stylus profilometer, and a constant erosion rate was assumed to convert sputtering time into sample depth. Implanted reference

TABLE I. Processing details and identification of the samples.

Wafer	Pretreatment	Na <sup>+</sup> dose (cm <sup>-2</sup> )	Postanneals 10 min O <sub>2</sub> (°C)
A_1		1 × 10 <sup>14</sup>	...
A_2		1 × 10 <sup>14</sup>	600
A_3		1 × 10 <sup>14</sup>	800
A_4		1 × 10 <sup>14</sup>	950
B_1		1 × 10 <sup>15</sup>	...
B_2		1 × 10 <sup>15</sup>	600
B_3		1 × 10 <sup>15</sup>	800
B_4		1 × 10 <sup>15</sup>	950
C_1	X	1 × 10 <sup>14</sup>	...
C_2	X	1 × 10 <sup>14</sup>	600
C_3	X	1 × 10 <sup>14</sup>	800
C_4	X	1 × 10 <sup>14</sup>	950
D_1	X	1 × 10 <sup>15</sup>	...
D_2	X	1 × 10 <sup>15</sup>	600
D_3	X	1 × 10 <sup>15</sup>	800
D_4	X	1 × 10 <sup>15</sup>	950

samples were used to quantify the Na and Li signals and for both elements, a detection limit in the low 10<sup>14</sup> cm<sup>-3</sup> range was obtained.

Open-volume defect evolution was monitored by positron annihilation spectroscopy (PAS). In PAS, positrons annihilate with electrons in a material and produce 511 keV gamma ( $\gamma$ ) radiation. Before the annihilation, positrons can be trapped by neutral or negatively charged open-volume defects or, in some cases, by negative ions. The trapping changes the annihilation characteristics, including Doppler broadening of the  $\gamma$  radiation. This broadening was measured using a Ge detector with an energy resolution of 1.24 keV. The broadened 511-keV-annihilation line is divided into two regions:  $S$  fraction of annihilations with low momentum electrons ( $p_L < 0.4$  a.u.) and  $W$  fraction of annihilations with high-momentum electrons ( $1.6$  a.u.  $< p_L < 4.0$  a.u.). Typically, the trapping of positrons at open-volume defects results in narrowing of the annihilation line.<sup>21</sup> The  $S$  parameter is more sensitive than  $W$  to changes in open volume of defects, thus in the course of presentation of the results, we emphasize on profiling of  $S$  parameters as a function of a positron implantation energy. However, the  $W$  parameter as a function of  $S$  parameter, i.e.,  $W$ - $S$  plots, are also presented. The positrons are introduced (implanted) into the samples in a form of a Makhov profile and the absolute width of the profile increases with increasing implantation energy. Thus, when converting positron energy to depth, the probed region has a considerable width around the mean positron penetration depth. Nominally, the  $R_p$  value of  $\sim 180$  nm corresponds to the mean penetration depth of 7.5 keV positrons. The maximum positron implantation energy used in this study was 36 keV corresponding to a mean penetration depth of  $\sim 2.2$   $\mu\text{m}$ .

### III. RESULTS

#### A. Li and Na concentration versus depth profiles

Li and Na concentration versus depth profiles for wafers A–D are shown in Figs. 1(a)–1(d), respectively, and they are found

to exhibit qualitatively different behavior. Firstly, competition between Na and Li occurs in wafers A and B upon the heat treatment, e.g., Li is depleted from the Na-rich region after 600 °C.<sup>22</sup> Subsequently, Li returns to this region when the Na concentration decreases at higher temperatures.<sup>23</sup>

In the wafer A, Fig. 1(a), a measurable Na diffusion is found at 800 °C (A\_3), while the redistribution of Li occurs already at 600 °C (A\_2), indicating Li/Na interaction at 600 °C or below.<sup>22</sup> The 800 °C anneal results in a boxlike Na profile with a plateau at  $\sim 4 \times 10^{17}$  cm<sup>-3</sup> (A\_3), characteristic of trap-limited diffusion (TLD), while the sample annealed at 950 °C (A\_4) exhibits a long Na tail resembling Fickian diffusion. For the wafer B, Fig. 1(b), the implantation dose is increased by one order of magnitude compared to that for wafer A, and the Na diffusion profiles extend to large depths. In addition, already the 600 °C anneal (B\_2) results in a significant redistribution of Na and not of Li only as in wafer A. Furthermore, the Na profiles in wafer B exhibit distinct plateaus around  $\sim 2$ – $5 \times 10^{17}$  Na/cm<sup>3</sup>, which increase in width with increasing annealing temperature.

In contrast, wafers C and D do not reveal any significant diffusion of Na into the sample bulk, Figs. 1(c) and 1(d). The Na atoms remain in the implanted region and then display a substantial surface out-diffusion at high temperatures. Further, Li does not show an anticorrelating behavior with Na, as for wafers A and B, but piles up in the implanted region of sample C\_2 (as observed also for other implanted elements).<sup>24</sup> However, for sample D\_2, Li does not pile up in this same region, most likely because the Li interaction with radiation-induced defects is blocked by higher concentration of Na atoms occupying vacancy-type defects (see Sec. III B). On the other hand, sample D\_3, demonstrates a depletion of Li from the mid-10<sup>15</sup> cm<sup>-3</sup> to the mid-10<sup>14</sup> cm<sup>-3</sup> range beyond the implanted region without any measurable Na diffusion. Interestingly, the 950 °C anneal results in approximately the same Na peak concentration ( $\sim 8 \times 10^{17}$  cm<sup>-3</sup>) for the samples C\_4 and D\_4, despite one order of magnitude difference in Na dose. This suggests that Na is trapped by defects present in the vicinity of the sample surface but not related to the implantation damage. The polishing procedure used for wafers C and D is known to cause subsurface defects, which progress into the sample during annealing and are stable up to 1100 °C.<sup>25</sup> Hence, the concentration of such defects expected to be identical in the wafers C and D, accounting for the fact that about the same concentration of Na is trapped irrespective of the implantation dose used.

#### B. Open-volume defect profiles

Figures 2(a)–2(d) display  $S$  parameters as a function of the positron implantation energy (as well as depth as a top axis) for wafers A–D, respectively, and Fig. 3 represents the corresponding  $W$ - $S$  plots. The data may be readily introduced if we group/discriminate between wafers A/B and C/D, similarly as in Sec. III A. Starting with wafer A, Fig. 2(a), the damage accumulated in the as-implanted sample (A\_1) is unveiled in the form of increase in  $S$  parameter. After annealing at 600 °C (A\_2), the further increase of the  $S$  parameter above the value characteristic of the Zn vacancy,  $S = 1.05 \times S_{\text{ZnORef}} = 0.439$ , indicates a formation of large open-volume defects

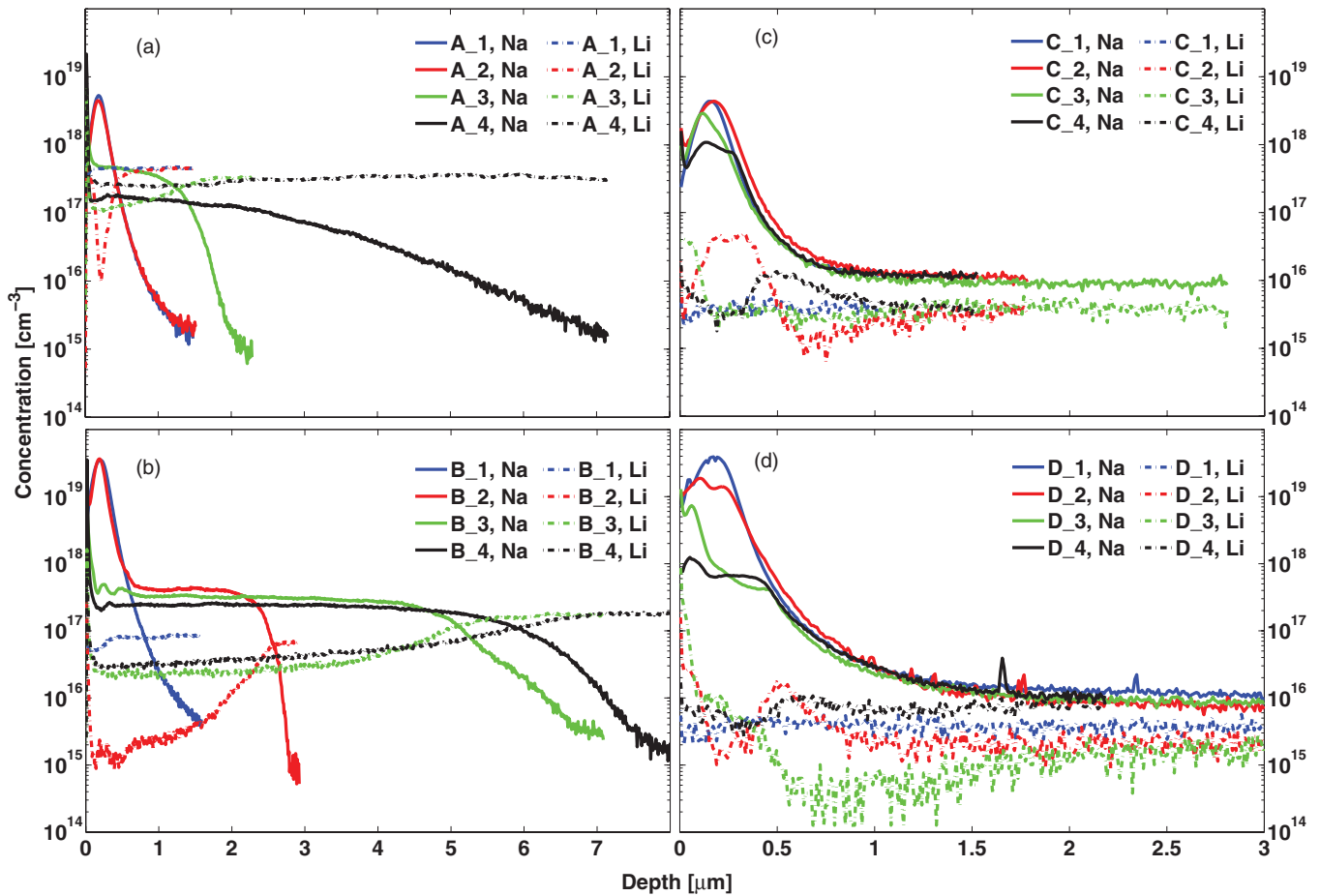


FIG. 1. (Color online) Na (solid) and Li (dot-dash) concentration vs depth profiles for wafers A–D [panels (a)–(d), respectively].

(vacancy clusters), consistent with previous implantation studies.<sup>24,26–30</sup> In terms of depth localization, the clustering occurs between the surface and  $R_p$ . Annealing of wafers A and B at temperatures above 600 °C decreases gradually the open-volume defect concentration to values below the PAS detection limit.

More information can be gained from the  $W$ - $S$  plot for wafer A in Fig. 3(a). The parameters are normalized to those of annihilation in the delocalized state in ZnO, labeled as “ZnO bulk” a vapor phase grown ZnO sample (ZnO in Fig. 2), with  $V_{Zn}$  concentration below the PAS detection limit, was measured as a reference simultaneously with the studied samples to give the “ZnO-bulk” point. Correspondingly, the “ $V_{Zn}$ ” point in Fig. 3 is based on positron saturation trapping in  $V_{Zn}$ ’s as measured in previous experiments.<sup>31–33</sup> If  $V_{Zn}$  is the dominating trap for positrons, all data points follow the  $V_{Zn}$  line and the position represents the actual  $V_{Zn}$  concentration. However, this is not the case in Li-rich samples, where the  $W$ - $S$  data converge below the  $V_{Zn}$  line due to positron trapping at  $Li_{Zn}$  as shown recently by Johansen *et al.*<sup>20</sup> A similar conclusion can also be drawn from Fig. 3(a) identifying the region just below the ZnO-bulk point, where our data converge ( $S \approx 1.005$ ,  $W \approx 0.95$ ), as the “HT-ZnO” point. It should be noted that the shift in “bulk”  $S$  and  $W$  values toward the HT-ZnO point complicates the estimation of the

$V_{Zn}$  concentration. However, when the data obey the  $V_{Zn}$  line, the  $V_{Zn}$  concentration can be deduced using previously obtained values for bulk and defect lifetimes<sup>31</sup> combined with the  $S$  and  $W$  parameters obtained in the present study.<sup>34</sup> In its turn, experimental data above the  $V_{Zn}$  line combined with high  $S$  parameter values indicate large (compared with  $V_{Zn}$ ) open-volume defects, i.e., vacancy clusters where both Zn and O atoms are missing, as clusters of only cation vacancies in compound semiconductors do not produce a deviation from the single vacancy line or its extension.<sup>35</sup> The defects in the as-implanted samples (e.g., A\_1) are clearly larger in size than a single  $V_{Zn}$ , and after annealing (A\_2), they evolve into even bigger vacancy clusters with a size of probably at least 3–5  $V_{Zn}$ ’s (and a corresponding amount of  $V_O$ ’s).<sup>36</sup> The results from sample A\_3 appear to be closer to the  $V_{Zn}$  line than the rest of the data, indicating a smaller contribution from  $Li_{Zn}$ , correlating with the Li redistribution in Fig. 1(a). In addition, high-temperature anneals remove a significant part of the implantation-induced defects and the data from sample A\_4 converge close to the HT-ZnO point.

The annealing behavior of the B samples, Figs. 2(b) and 3(b), reveals intriguing characteristics to be attributed to the higher Na dose as compared to that for wafer A. In Fig. 2(b), a large reduction of the implantation damage occurs already at 600 °C (B\_2) followed by further annealing after the 800 °C

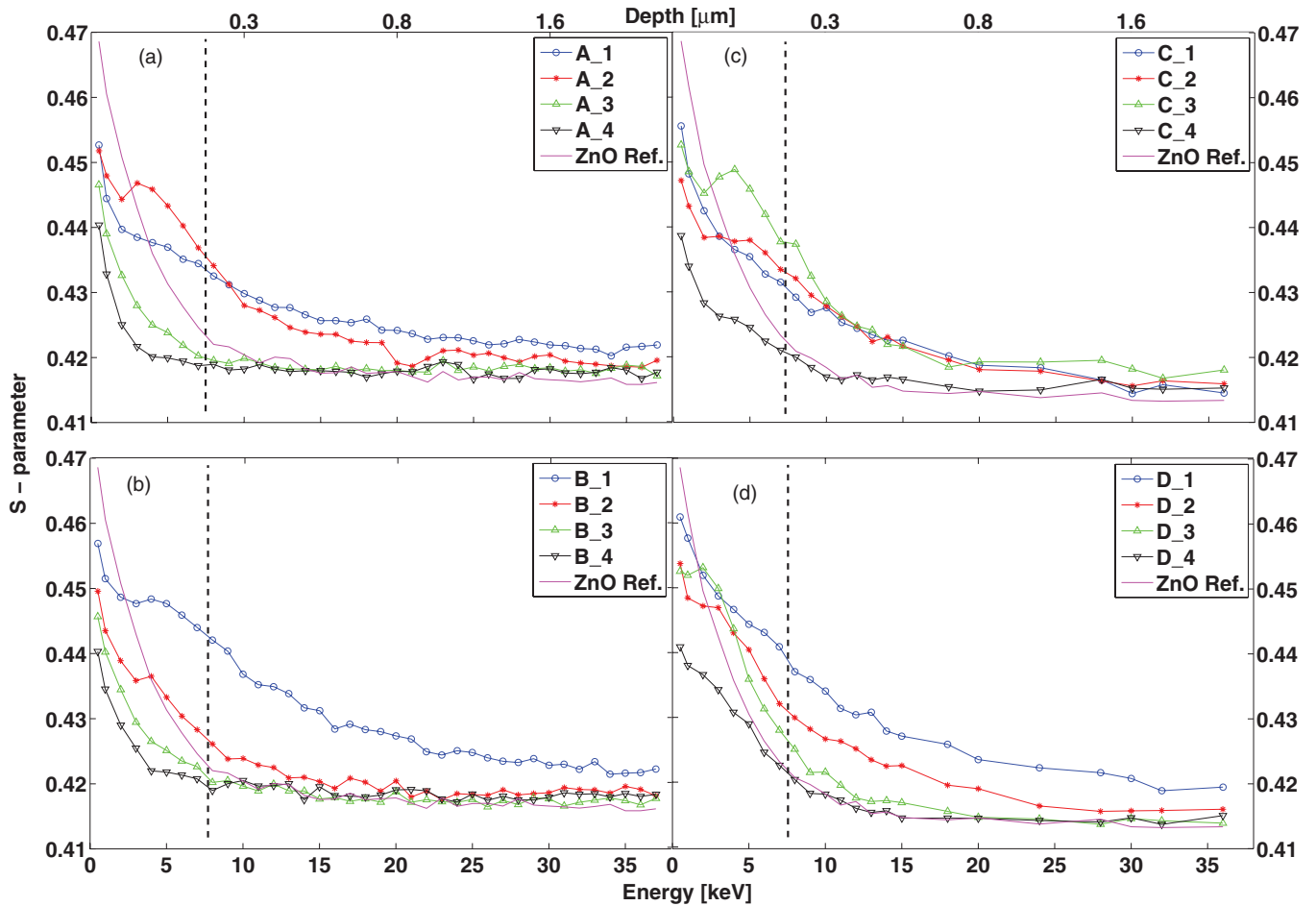


FIG. 2. (Color online)  $S$  parameter as a function of positron implantation energy/depth for wafers A–D plotted in panels (a)–(d), respectively. The dashed lines indicate the projected range of the Na implants.

and 950 °C treatment (B.3 and B.4, respectively). Here, it is worth noting that the redistribution of Na occurring in B.2 [see Fig. 1(b)] does not take place in A.2 [see Fig. 1(a)]. Consistent with the previous discussion, in  $W$ - $S$  data for B.1, Fig. 3(b), yield a slope directed toward the HT-ZnO point while for B.2 the slope is shifted toward the ZnO-bulk point. For B.3, the data converge close to the ZnO-bulk point, indicating a low content of open-volume defects. Further increase of the temperature shifts the data (B.4) closer to the HT-ZnO point, in accordance with decreasing/increasing Na/Li concentrations, respectively [cf. Fig. 1(b)]. For B.3, the body of the data obey the  $V_{Zn}$  line and the  $V_{Zn}$  concentration is estimated<sup>31</sup> to be  $\sim 7 \times 10^{15} \text{ cm}^{-3}$ . The short positron diffusion length, indicated by the rapid decrease of the  $S$  parameter from surface to bulk value [e.g., A.4 and B.4 in Figs. 2(a) and 2(b)], suggests the presence of negatively charged ions with annihilation parameters similar to the ZnO lattice, possibly  $\text{Na}_{Zn}^-$ .

Qualitatively different behavior is observed in wafers C and D. Specifically, in wafer C, annealing at 600 (C.2) and 800 °C (C.3) leads to clustering of vacancies, mainly in the surface tail of the damage profile. The clusters are partly removed by the 950 °C anneal (C.4), but some defects still remain, evidenced by the change in the slope of the  $S$ -parameter curve after the first few data points from the surface [both in Figs. 2(c) and 2(d)].

In accordance with the fact that the preanneals at 1500 °C reduce the Li concentration to the  $10^{15} \text{ cm}^{-3}$  range, all the data slopes in Figs. 3(c) and 3(d) are directed toward the ZnO-bulk point and the  $V_{Zn}$  concentrations are estimated to be  $\sim 1.4 \times 10^{16}$  and  $\sim 7 \times 10^{15} \text{ cm}^{-3}$  in samples C.4 and D.3, respectively. It should be noted that even if the difference between the samples C.4 and D.3 is small, it is statistically significant. A detailed examination of Figs. 3(c) and 3(d) unveils that the D.3 data are close to the ZnO reference point, while the C.4 data are clearly shifted toward the  $V_{Zn}$  point. The near surface defects responsible for the large deviation from the  $V_{Zn}$  line in Fig. 3(c) and 3(d), are attributed to the polishing process,<sup>25</sup> and the similarity between polishing- and implantation-induced defects has also been observed previously by other authors.<sup>37</sup> In contrast, for wafer D, the  $S$  parameter decreases monotonously at  $R_p$  with increasing temperature, Fig. 2(d), which is presumably to be associated with the increased presence of Na.

## IV. DISCUSSION

### A. Na configurations and its interplay with Li in ZnO

Park *et al.*<sup>17</sup> and Wardle *et al.*<sup>18</sup> have calculated the formation energies for interstitial and substitutional Li and Na ( $\text{Li}_i$ ,

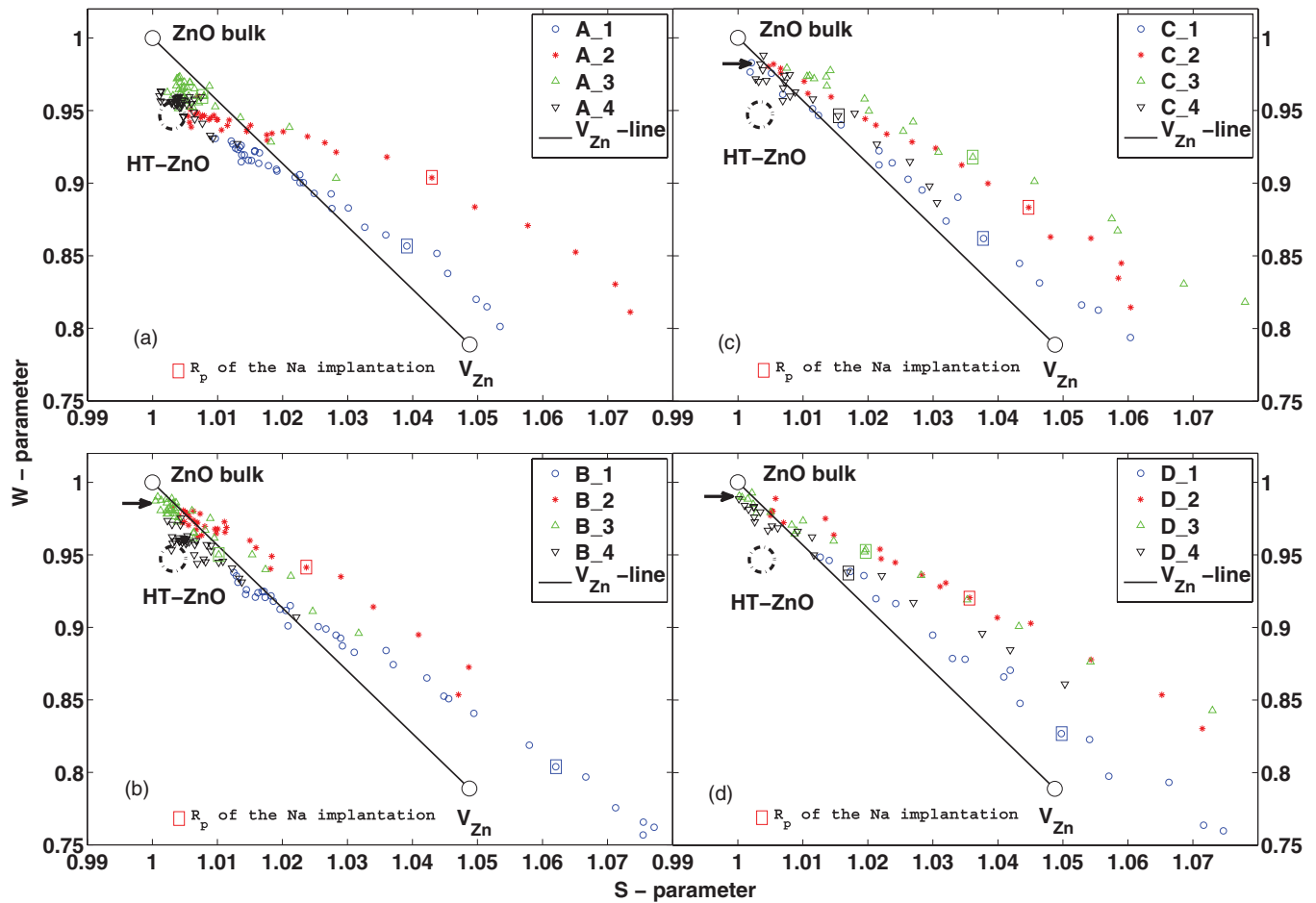


FIG. 3. (Color online)  $W$ - $S$  plots for wafers A–D [(a)–(d) panels, respectively]. The arrows indicate the regions used to evaluate the  $V_{Zn}$  concentrations. The data points marked with squares correspond to a positron implantation energy of  $\sim 8$  keV, so that the mean penetration depth corresponds to the  $R_p$ . Surface related annihilation points have been omitted for clarity.

$Li_{Zn}$ , and  $Na_i$ ,  $Na_{Zn}$ , respectively) as a function of  $E_F$ . Their results show that the concentration of  $Li_{Zn}$  ( $Na_{Zn}$ ) prevails over the concentration of  $Li_i$  ( $Na_i$ )—meaning the defect has a lower formation energy—when  $E_F$  is close to the conduction band edge, but  $Li_i$  ( $Na_i$ ) becomes favorable when  $E_F$  moves toward the valence band edge. Formation energies ( $E_{form}$ ) of interstitial and substitutional Li (Na) are intersecting around the middle of the band gap, resulting in a self-compensation and thus highly resistive, but still  $n$ -type, material. Wardle *et al.*<sup>18</sup> also predicted that Na would be more stable on a zinc site as compared to Li, which has been experimentally confirmed.<sup>22</sup> Since  $E_{form}(Na_{Zn}) + E_{form}(Li_i) < E_{form}(Na_i) + E_{form}(Li_{Zn})$ ,  $Na_i$  causes  $Li_{Zn}$  to change the configuration to  $Li_i$ , which will diffuse and eventually get trapped in the sample bulk.

The same interplay between Na and Li as discussed in Ref. 22 can be seen in Figs. 1(a) and 1(b). Nevertheless, at higher temperatures ( $\gtrsim 800^\circ\text{C}$ ), a significant amount of Li is observed in the Na enriched regions, indicating that not all the available trap sites are occupied by Na. This can be due to a high dissociation rate of the Na-trap complex or that the diffusion source of Na is exhausted. The Na plateau level exceeds the HT-Li level (which most likely represents the equilibrium concentration during sample growth) by a factor

of  $\sim 2$  in wafers A and B. The difference between the bulk level of Li and plateau levels of Na in samples B.2 and B.3 can be attributed to a 50–60 meV difference between the formation energies of  $Li_{Zn}$  and  $Na_{Zn}$ , assuming equilibrium conditions and no other limiting factors such as the supply of Li and Na or changes in  $E_F$ .

The Li concentration in Figs. 1(c) and 1(d) (wafers C and D) is  $\sim 10^{-2} \times$  HT-Li, and the behavior of Na and Li are very different relative to those in Figs. 1(a) and 1(b). In the C and D samples, the Li redistribution resembles that when other elements than Na are implanted, and may be explained in terms of evolution of the implantation-induced damage.<sup>24</sup> Notably, no Na redistribution above the background level is observed but only a reduction in the peak concentration, indicating strong out-diffusion through the surface. If the concentration of Na incorporated beyond the implanted region would be determined by the  $Na_{Zn}$  formation energy, one would expect similar concentrations in diffusion tails for wafers C and D as for wafers A and B provided that the  $E_F$  position is the same. However,  $E_F$  is high in the bulk of wafers C and D due to the lower Li concentration remaining after preannealing at  $1500^\circ\text{C}$ .<sup>19</sup> Hence the concentration of  $Na_i$ , assumed to be the mobile species, is highly suppressed in the bulk of wafers C and D and out-diffusion via the surface prevails. However, it

is likely that a low diffusion flux of Na<sub>i</sub> toward the bulk still exists, as corroborated by the depletion of Li from the mid-10<sup>15</sup> to the mid-10<sup>14</sup> cm<sup>-3</sup> range in depth interval ~0.5–1.5 μm for sample D\_3, Fig. 1(d).

### B. Evolution of open-volume defects after Na implantation

The effect of Na on the evolution of open-volume defects is illustrated by Figs. 2(a) and 2(b) (wafers A and B, respectively). For wafer A, the *S* parameter increases first and then decreases with increasing temperature, while for wafer B, the *S* parameter decreases monotonously with increasing temperature. Hence, in wafer A, vacancies form large clusters at 600 °C, which then dissociate at higher temperature. However, such clustering of the vacancies is not observed in wafer B, which contains a factor of ten higher concentration of Na. A comparison of Figs. 3(a) and 3(b) shows that the data from wafer B are close to the ZnO-bulk point, while the data from wafer A are close to the HT-ZnO point.<sup>20</sup> Altogether, these results provide strong evidence for a reduction in the open volume of defects due to the presence of Na and more specifically due to the substitution of Li<sub>Zn</sub> by Na<sub>Zn</sub> at temperatures ≥600 °C. It can be noted that even if the Li-related positron signal is clearly stronger in the A than in the B samples, sample B\_4 seems to exhibit a noticeable Li signal. This may be due to the subtle balance between Na and Li concentrations in the region probed by the positrons: [Na]/[Li] ~ 20 in sample B\_3, while it is only ~5 in sample B\_4 ([Na]/[Li] ~ 1–5 in the A samples) (brackets denote concentration values).

The PAS data for wafers C and D, [Figs. 2(c)–2(d) and 3(c)–3(d)] corroborate the evidence of Li<sub>Zn</sub> to Na<sub>Zn</sub> substitution in spite of the presence of residual polishing-induced defects remaining in the vicinity of the surface. Indeed, the trend of the *S* parameter at depths around R<sub>p</sub> in wafer C is the same as for wafer A—first an increase and then a decrease as a function of temperature—and wafer D [see Fig. 2(d)] is similar to wafer B—decreasing monotonously as a function of temperature. All the data in Figs. 3(c) and 3(d) are aligned with the ZnO-bulk point and fall on, or above, the V<sub>Zn</sub> line fully consistent with the fact that the pretreatment at 1500 °C removes Li. In addition, in wafer D (high Na dose), the data converge closer to the ZnO-bulk point than in wafer C, showing smaller concentration of open-volume defects.

For wafer A, the V<sub>Zn</sub> concentration cannot be deduced from the PAS data because of the strong contribution from Li<sub>Zn</sub>.<sup>20,31</sup> However, the data from wafers B (B\_3), C (C\_4), and D (D\_3) can be used and the corresponding V<sub>Zn</sub> contents are 7 × 10<sup>15</sup>, 1.4 × 10<sup>16</sup>, and 7 × 10<sup>15</sup> cm<sup>-3</sup>, respectively, where the influence by negatively charged impurities is neglected, as discussed previously.<sup>34</sup> Assuming that equilibrium conditions apply during the annealing and that the V<sub>Zn</sub>'s are stable during cooling down, the following formation energies of V<sub>Zn</sub> are obtained in these three samples: 1.44, 1.57, and 1.44 eV, respectively. According to theoretical estimates,<sup>9</sup> these values imply that the samples are somewhat Zn rich.

### C. Migration and trapping of Na

For wafers A and B [see Figs. 1(a) and 1(b)], Na migrates during the post implantation annealing with a clear diffusion

tail already at 600 °C for wafer B (B\_2) but not for wafer A (A\_2). This is in accordance with a higher absolute amount of Na on lightly bound sites immediately after the implantation for wafer B, due to the higher Na dose, suggesting Na<sub>i</sub>'s to be the diffusing species. The diffusion profiles for wafer B show characteristic TLD exhibiting a plateau level in the range of ~2–5 × 10<sup>17</sup> Na/cm<sup>3</sup>, which decreases with increasing temperature. Also in wafer A, the plateau level as well as the implantation peak decrease rapidly, and sample A\_4 displays a profile resembling a solution of Fick's equation, equivalent to a dissociation-dominated TLD process. For all the samples displaying Na diffusion, the previously discussed interplay between Li and Na occurs in the Na-rich regions, corroborating that Li and Na compete for the same traps.

In wafers C and D [see Figs. 1(c) and 1(d)], the most striking feature is the absence of redistribution of the implanted Na, demonstrating the pronounced effect of the preannealing at 1500 °C on the migration process of Na. The preannealing decreases the Li concentration [as well as increases the Na concentration but in negligible amount compared with the Na contents in the diffusion tails in Figs. 1(a) and 1(b)], and there are at least three possible scenarios for the evolution of the TLD process of Na: (i) the nature of the traps is the same for Li and Na, and they are strongly reduced in concentration during the pretreatment, (ii) Li<sub>Zn</sub> is the trap for the diffusing Na, and/or (iii) the Na flux is greatly reduced by the pretreatment (see discussion in Sec. IV A).

The strong interplay between Li and Na, and the reduction in concentration of open-volume defects in Na-rich regions show that Li<sub>Zn</sub> is, indeed, a trap for the diffusing Na species. This can occur via, for instance, the reaction Na<sub>i</sub><sup>+</sup> + Li<sub>Zn</sub><sup>-</sup> → Na<sub>Zn</sub><sup>-</sup> + Li<sub>i</sub><sup>+</sup> in which the released Li<sub>i</sub>'s are highly mobile and subsequently would be trapped in the bulk through the reaction Li<sub>i</sub><sup>+</sup> + V<sub>Zn</sub><sup>2-</sup> → Li<sub>Zn</sub><sup>-</sup> (other reactions are also possible, including pair formation Li<sub>i</sub> – Li<sub>Zn</sub>).<sup>18</sup> However, this can not explain why the Na concentration exceeds the HT-Li level in samples A\_3 and B\_2–B\_4, so an additional process must take place. Under equilibrium conditions, V<sub>Zn</sub> is maintained and in *n*-type samples, the Na concentration is to a large extent anticipated to be controlled by the formation energy of Na<sub>Zn</sub>; as discussed in Sec. IV A, a value lower by only ~50 meV than that of Li<sub>Zn</sub> accounts for the difference between the HT-Li level and the Na plateau level in the samples A\_3 and B\_2–B\_4. Thus the reaction Na<sub>i</sub><sup>+</sup> + V<sub>Zn</sub><sup>2-</sup> → Na<sub>Zn</sub><sup>-</sup> is regarded as highly plausible.

## V. CONCLUSIONS

In conclusion, SIMS and PAS have been applied to study impurity migration and evolution of open-volume defects in Na<sup>+</sup> implanted HT-ZnO samples. In contrast to most other elements, the presence of Na decreases the concentration of open-volume defects upon post-implant annealing and at temperatures exceeding 600 °C, Na redistributes in a trap-limited diffusion mode correlating with the concentration of Li. A dominating trap for the migrating Na atoms is substitutional Li (Li<sub>Zn</sub>), most likely via the reaction Na<sub>i</sub><sup>+</sup> + Li<sub>Zn</sub><sup>-</sup> → Na<sub>Zn</sub><sup>-</sup> + Li<sub>i</sub><sup>+</sup>, as supported by theoretical estimates of formation energies. However, this process is not sufficient to explain all the experimental observations and zinc vacancies

are also believed to contribute to the Na trapping via the  $\text{Na}_i^+ + \text{V}_{\text{Zn}}^{2-} \rightarrow \text{Na}_{\text{Zn}}^-$  reaction; assuming the formation energy of  $\text{Na}_{\text{Zn}}$  to be  $\sim 50$  meV lower than that of  $\text{Li}_{\text{Zn}}$ , this reaction accounts for the fact that the Na concentration can exceed the bulk (equilibrium) Li concentration by about a factor of two.

## ACKNOWLEDGMENTS

The authors gratefully acknowledge the financial support from the Norwegian Research Council through the NANOMAT, FRIENERGI, and FRINAT programs, the Academy of Finland, and NordForsk.

\*p.t.neuvonen@smn.uio.no

- <sup>1</sup>D. G. Thomas, *J. Phys. Chem. Solids* **15**, 86 (1960).
- <sup>2</sup>Y. R. Ryu, T. S. Lee, J. A. Lubguba, H. W. White, Y. S. Park, and C. J. Youn, *Appl. Phys. Lett.* **87**, 153504 (2005).
- <sup>3</sup>A. Tsukazaki, M. Kubota, A. Ohtomo, T. Onuma, K. Ohtani, H. Ohno, S. F. Chichibu, and M. Kawasaki, *Jpn. J. Appl. Phys.* **44**, L643 (2005).
- <sup>4</sup>D. C. Reynolds, C. W. Litton, D. C. Look, J. E. Hoelscher, B. Claffin, T. C. Collins, J. Nause, and B. Nemeth, *J. Appl. Phys.* **95**, 4802 (2004).
- <sup>5</sup>K. Maeda, M. Sato, I. Niikura, and T. Fukuda, *Semicond. Sci. Technol.* **20**, S49 (2005).
- <sup>6</sup>S. E. Harrison, *Phys. Rev.* **93**, 52 (1954).
- <sup>7</sup>A. R. Hutson, *Phys. Rev.* **108**, 222 (1957).
- <sup>8</sup>A. F. Kohan, G. Ceder, D. Morgan, and C. G. Van de Walle, *Phys. Rev. B* **61**, 15019 (2000).
- <sup>9</sup>A. Janotti and C. G. van de Walle, *Phys. Rev. B* **76**, 165202 (2007).
- <sup>10</sup>A. Janotti and C. G. van de Walle, *Appl. Phys. Lett.* **87**, 122102 (2005).
- <sup>11</sup>R. Schifano, E. V. Monakhov, L. Vines, B. G. Svensson, W. Mtangi, and F. D. Auret, *J. Appl. Phys.* **106**, 043706 (2009).
- <sup>12</sup>E. V. Monakhov, A. Yu. Kuznetsov, and B. G. Svensson, *J. Phys. D* **42**, 153001 (2009).
- <sup>13</sup>C. G. van de Walle, *Phys. Rev. Lett.* **85**, 1012 (2000).
- <sup>14</sup>A. Janotti and C. G. van de Walle, *Rep. Prog. Phys.* **72**, 126501 (2009).
- <sup>15</sup>S. B. Zhang, S.-H. Wei, and A. Zunger, *J. Appl. Phys.* **83**, 3192 (1998).
- <sup>16</sup>S.-H. Wei and S. B. Zhang, *Phys. Rev. B* **66**, 155211 (2002).
- <sup>17</sup>C. H. Park, S. B. Zhang, and S.-H. Wei, *Phys. Rev. B* **66**, 073202 (2002).
- <sup>18</sup>M. G. Wardle, J. P. Goss, and P. R. Briddon, *Phys. Rev. B* **71**, 155205 (2005).
- <sup>19</sup>B. G. Svensson, T. M. Børseth, K. M. Johansen, T. Maqsood, R. Schifano, U. Grossner, J. S. Christensen, L. Vines, P. Klason, Q. X. Zhao *et al.*, *Mater. Res. Soc. Symp. Proc.* **1035**, L04–01 (2008).
- <sup>20</sup>K. M. Johansen, A. Zubiaga, I. Makkonen, F. Tuomisto, P. T. Neuvonen, K. E. Knutsen, E. V. Monakhov, A. Yu. Kuznetsov, and B. G. Svensson, *Phys. Rev. B* **83**, 245208 (2011).
- <sup>21</sup>K. Saarinen, P. Hautojärvi, and C. Corbel, *Identification of Defects in Semiconductors* (Elsevier, 1998), Vol. 51. ISBN 0080-8784.
- <sup>22</sup>P. T. Neuvonen, L. Vines, A. Yu. Kuznetsov, B. G. Svensson, X. L. Du, F. Tuomisto, and A. Hallén, *Appl. Phys. Lett.* **95**, 242111 (2009).
- <sup>23</sup>Note that an apparent difference in Li background concentration between B\_1 and B\_2 and the rest of the A and B samples in Figs. 1(a) and 1(b) is because samples B\_1 and B\_2 were measured under different conditions causing some charge buildup affecting the calibration of Li-related signals. The actual background Li content is expected to be the same as in all B-type samples, more specifically in the range of  $2\text{--}4 \times 10^{17} \text{ cm}^{-3}$ . However, no normalization was made because it did not affect the interpretations.
- <sup>24</sup>T. Moe Børseth, F. Tuomisto, J. S. Christensen, E. V. Monakhov, B. G. Svensson, and A. Yu. Kuznetsov, *Phys. Rev. B* **77**, 045204 (2008).
- <sup>25</sup>F. A. Selim, M. H. Weber, D. Solodovnikov, and K. G. Lynn, *Phys. Rev. Lett.* **99**, 085502 (2007).
- <sup>26</sup>Z. Q. Chen, T. Sekiguchi, X. L. Yuan, M. Maekawa, and A. Kawasuso, *J. Phys. Condens. Matter* **16**, S293 (2004).
- <sup>27</sup>Z. Q. Chen, M. Maekawa, S. Yamamoto, A. Kawasuso, X. L. Yuan, T. Sekiguchi, R. Suzuki, and T. Ohdaira, *Phys. Rev. B* **69**, 035210 (2004).
- <sup>28</sup>Z. Q. Chen, M. Maekawa, A. Kawasuso, R. Suzuki, and T. Ohdaira, *Appl. Phys. Lett.* **87**, 091910 (2005).
- <sup>29</sup>Z. Q. Chen, M. Maekawa, A. Kawasuso, S. Sakai, and H. Naramoto, *J. Appl. Phys.* **99**, 093507 (2006).
- <sup>30</sup>Z. Q. Chen, M. Maekawa, A. Kawasuso, and H. Naramoto, *Phys. Status Solidi C* **4**, 3646 (2007).
- <sup>31</sup>F. Tuomisto, V. Ranki, K. Saarinen, and D. C. Look, *Phys. Rev. Lett.* **91**, 205502 (2003).
- <sup>32</sup>F. Tuomisto, K. Saarinen, D. C. Look, and G. C. Farlow, *Phys. Rev. B* **72**, 085206 (2005).
- <sup>33</sup>A. Zubiaga, F. Tuomisto, V. A. Coleman, H. H. Tan, C. Jagadish, K. Koike, S. Sasa, M. Inoue, and M. Yano, *Phys. Rev. B* **78**, 035125 (2008).
- <sup>34</sup>The possible presence of negatively charged ions is not accounted for and causes an underestimation of the  $V_{\text{Zn}}$  concentration.<sup>24</sup>
- <sup>35</sup>C. Rauch, I. Makkonen, and F. Tuomisto, *Phys. Rev. B* **84**, 125201 (2011).
- <sup>36</sup>T. Moe Børseth, F. Tuomisto, J. S. Christensen, W. Skorupa, E. V. Monakhov, B. G. Svensson, and A. Yu. Kuznetsov, *Phys. Rev. B* **74**, 161202 (2006).
- <sup>37</sup>M. H. Weber, F. A. Selim, D. Solodovnikov, and K. G. Lynn, *Appl. Surf. Sci.* **255**, 68 (2008).